MULTI-WAVELENGTH RADIO CONTINUUM EMISSION STUDIES OF DUST-FREE RED GIANTS

Eamon O'Gorman[1], Graham M. Harper[1], Alexander Brown[2], Stephen Drake[3], and Anita M.S. Richards[4]
Draft version March 30, 2013

ABSTRACT

Multi-wavelength centimeter continuum observations of non-dusty red giants directly sample their wind acceleration zones where most of the energy that drives their mass loss is being deposited. These stars are feeble thermal emitters at these wavelengths however, and previous observations have provided only a small number of modest signal-to-noise measurements accumulated over many years. Here, we present multi-wavelength Karl G. Jansky Very Large Array (VLA) thermal continuum observations of the acceleration zones of two dust-free red giants, Arcturus (α Boo: K2 III) and Aldebaran (α Tau: K5 III). Uniquely, our observations were mostly carried out within a few days of each other so any long term variability that may exist can be ignored. We report the first detections at many wavelengths for each star including a detection at 10 cm (3.0 GHz; S-band) for both stars and a 20 cm (1.5 GHz; L-band) detection for α Boo. This is the first time single (non-binary) luminosity class III red giants have been observed at such long continuum wavelengths. These long wavelength flux density measurements sample the outer layers of the stars atmosphere where the wind velocity is approaching (or possibly has reached) its terminal value and the ionization balance is becoming frozen-in. As a result, they are important empirical inputs for future atmospheric models. We present spectral energy distributions for both stars and compare these with previous measurements and published semi-empirical models based on ultraviolet data. The marked deviations between our data and existing semi-empirical models highlight the need for new atmospheric models to be developed. The derived spectral indices are discussed in relation to the possible properties of the stellar atmospheres and a simple analytical atmospheric model is developed for α Boo's outer atmosphere which is in good agreement with our new long wavelength flux densities.

Keywords: circumstellar matter — Stars: individual: (α Boo, α Tau) — Stars: late-type — Stars: chromospheres — Stars: winds, outflows — Radio continuum: stars

1. INTRODUCTION

Mass loss from late-type evolved stars plays a crucial role in both stellar and galactic evolution and ultimately provides part of of the material required for the next generation of stars and planets. Despite the importance of this phenomenon and decades of study, the mechanisms that drive winds from evolved spectral-type K through mid-M stars remain an enduring mystery [clearly laid out by Holzer & MacGregor (1985) but still unsolved, e.g., Crowley et al. 2009]. There is insufficient atomic, molecular, or dust opacity to drive a radiation-driven outflow and acoustic/pulsation models cannot drive the observed mass loss rates (Sutmann & Cuntz 1995). Optical and ultraviolet observations reveal an absence of hot wind plasma and the winds are thus too cool to be Parker-type thermally-driven flows (e.g., Linsky & Haisch 1979; Ayres et al. 1981).

Magnetic fields are most likely involved in the mass loss process, although current magnetic models are also unsuccessful. Exquisite high signal-to-noise (S/N) ratio *Hubble* ultraviolet (UV) spectra have revealed that the 1-D linear Alfvén wave-driven wind models of the 1980s (e.g., Hartmann & MacGregor 1980) are unten-

able. These models predict chromospheres as integral parts of turbulently extended and heated wind acceleration zones, but the theoretical line profiles and electron densities do not agree with the *Hubble* spectra, e.g., Judge & Carpenter (1998). One important property of cool evolved star winds gleaned from UV spectra is that, for the most part, the red giant winds accelerate in a quasi-steady manner and are not the result of ballistic ejecta. A new generation of theoretical models with outflows driven within diverging magnetic flux tubes have now emerged (Falceta-Gonçalves et al. 2006; Suzuki 2007) but these too are not yet in agreement with observations (Crowley et al. 2009). It has also been suggested that the winds may be driven by some form of magnetic pressure acting on very highly clumped wind material (Eaton 2008) but Harper (2010) does not find support for this hypothesis. Progress in this field continues to be driven by observations that provide new insights into the mass loss problem.

1.1. *Radio Continuum Observations*

Although studies of wind-scattered UV and optical line profiles have provided clues to the mass loss rates and radial distribution of the mean and turbulent velocity fields, the thermal structure remains poorly constrained. In the UV, the source function is very sensitive to electron temperature (i.e., $S_\nu \propto e^{-h\nu/kT}$) and so a localized hot plasma component in a dynamic atmosphere can completely dominate the temporally and spatially averaged emission and not reflect the global mean value. At

[1] School of Physics, Trinity College Dublin, Dublin 2, Ireland
[2] Center for Astrophysics and Space Astronomy, University of Colorado, 389 UCB, Boulder, CO 80309, USA
[3] NASA Goddard Space Flight Center, Greenbelt, MD 20771, USA
[4] Jodrell Bank Centre for Astrophysics, School of Physics and Astronomy, University of Manchester, Manchester M13 9PL, UK

radio wavelengths however, the source function is thermal and is just the Rayleigh-Jeans tail of the Planck function, which is linear in electron temperature (i.e., $S_\nu = 2kT\nu^2/c^2$) and so should give a more appropriate estimate of the thermal radial wind structure. It is this value that controls the atomic level populations and ionization that feed into UV spectroscopic analyses. This value is also needed to quantify the implied thermal heating supplied to the wind by the unknown driving source/sources, and thus derive constraints on potential mass loss mechanisms.

In the cm-radio regime the radio opacity strongly increases with wavelength (i.e., $\kappa_\lambda \propto \lambda^{2.1}$) and so the longer wavelengths sample the extended layers of the stars atmosphere, thus essentially providing us with spatial information about the star's mass outflow region. The thermodynamic properties in this spatial region control the ionization in the far wind because the ionization balance, which also controls the cooling rates, becomes *frozen-in* at these radii due to advection. Furthermore, it is these outer extended regions of the star's atmosphere that contribute to the commonly seen P Cygni line profiles in the UV. In these profiles the line-of-sight absorption caused by the star's wind is superimposed on the blueshifted emission. Thus, centimeter radio continuum observations can provide a test of models based on these UV profiles. In this paper we directly compare our new NRAO[5] Karl G. Jansky Very Large Array (VLA) observations with atmospheric models derived from UV analysis.

1.2. *Sample Selection*

Currently the most detailed spatial information about the atmospheres of K and early M evolved stars is obtained from eclipsing binaries such as the symbiotic and ζ Aurigae systems (e.g., Baade et al. 1996; Eaton 2008; Crowley et al. 2008). Even though these systems offer us the best opportunity to obtain information on the dynamics and thermodynamics at various heights in the evolved star's atmosphere, the very nature of the binary system may introduce further complexities. For example, the orbital separation is often within the wind acceleration region and one could expect flow perturbations to be present (e.g., Chapman 1981). In fact, using the 'old' VLA, Harper et al. (2005) confirm that the velocity structure of of ζ Aurigae is not typical of single stars with similar spectral types, such as λ Velorum (Carpenter et al. 1999).

In order to avoid the assumed additional complexities of a companion, we have selected two single luminosity class III red giants: Arcturus (α Boo: K2 III) and Aldebaren (α Tau: K5 III). These nearby red giants have been extensively studied at other wavelengths and their stellar parameters, which are briefly summarized in Table 1, are accurately known. These stars are predicted to be point sources at all frequencies in all VLA configurations so our radio observations measure their total flux density, F_ν. Moreover, both stars have existing semi-empirical 1-D chromospheric and wind models which we directly compare to our data in this paper.

Table 1
Some properties of our red giant sample.

	α Boo	α Tau
Spectral Type	K2 III	K5 III
Effective Temperature (K)	4294 ± 30	3970 ± 49
Angular Diameter (mas)	21.0 ± 0.2	20.2 ± 0.3
Distance (pc)	11.3 ± 0.1	20.4 ± 0.3
Radius ($R_\odot$)	25.4 ± 0.3	44.4 ± 1.0
Mass Loss Rate ($M_\odot$ yr^{-1})	2×10^{-10}	1.6×10^{-11}
Wind Temperature (K)	$\sim 10,000$	$< 10,000$
Wind Terminal Velocity	~ 40 km s^{-1}	~ 30 km s^{-1}
Semi-empirical model	Drake (1985)	McMurry (1999)

Note. — Effective temperatures and photospheric angular diameters are from di Benedetto (1993). Distances are from van Leeuwen (2007). Mass loss rates are from Drake (1985) and Robinson et al. (1998).

2. OBSERVATIONS AND DATA REDUCTION

Observations of α Boo and α Tau were carried out with the VLA during February 2011 at Q, Ka, K, X, C, and S-band in B-configuration (PI: Harper; program 10C-105). α Boo was also observed at S and L-band in July 2012 when the VLA was again in B-configuration (PI: O'Gorman; program 12A-472). Some details of these observations are given in Table 2. For the 2011 observations, the correlator was set up with two 128 MHz sub-bands centered on the frequencies listed in Table 2. Each sub-band had sixty-four channels of width 2 MHz and four polarization products (RR, LL, RL, LR). For the S and L-band observations in 2012, the 1-2 GHz and 2-4 GHz frequency ranges were both divided into 16 sub-bands, each with sixty-four channels. The channel width was 2 and 1 MHz for S and L-band, respectively.

Both α Boo and α Tau were slightly offset from the phase-center by ∼5 synthesized beam widths in order to avoid possible errors at phase-center. All scheduling blocks (SBs) were kept to ≤ 2.5 hours of duration to improve their likelihood of being scheduled. For the high frequency observations (i.e., Q, Ka, and K-bands) we used the *fast switching* technique which consisted of rapidly alternating observations of the target source and a nearby unresolved phase calibrator. The total cycle times for the Q, Ka, and K-band observations were 160, 230, and 290 s, respectively. For both target sources these high frequency observations were combined into a single 2 hour observing track and commenced with X-band reference pointing with solutions being applied on-line. After X-band pointing the target source was observed at Q-band to insure the best pointing solutions were used. The lower frequencies tracks were composed of repeatedly interleaving observations of the target source and a nearby phase calibrator but had much longer cycle times. The primary calibration sources 3C286 and 3C138 were observed at the end of all tracks and were used to measure the complex bandpass and set the absolute flux for α Boo and α Tau, respectively.

The data were flagged, calibrated, and imaged within the Common Astronomical Software Application (CASA; McMullin et al. 2007) package. Data deemed to be bad by the VLA online system were flagged, as were pure zeros, non-operational antennae, dummy scans at the beginning of each track, and poorly performing an-

Table 2
VLA Observations

Star	Date	Band	Frequency[a] (GHz)	Wavelength (cm)	Time on Star (hr)	Bandwidth (GHz)	Number of Antennae[b]	Phase Calibrator
α Boo	2011 Feb 22	Q	43.3	0.7	0.3	0.256	22	J1357+1919
α Boo	2011 Feb 22	Ka	33.6	0.9	0.2	0.256	23	J1357+1919
α Boo	2011 Feb 22	K	22.5	1.3	0.4	0.256	24	J1357+1919
α Boo	2011 Feb 11	X	8.5	3.5	0.3	0.256	18	J1415+1320
α Boo	2011 Feb 11	C	5.0	6.0	0.5	0.256	21	J1415+1320
α Boo	2011 Feb 13	S	3.1	9.5	1.8	0.256	12	J1415+1320
α Boo	2012 Jul 19	S	3.0	10.0	0.7	2.0	23	J1415+1320
α Boo	2012 Jul 20	L	1.5	20.0	1.6	1.0	23	J1415+1320
α Tau	2011 Feb 11	Q	43.3	0.7	0.3	0.256	22	J0431+1731
α Tau	2011 Feb 11	Ka	33.6	0.9	0.2	0.256	19	J0449+1121
α Tau	2011 Feb 11	K	22.5	1.3	0.4	0.256	21	J0449+1121
α Tau	2011 Feb 13	X	8.5	3.5	0.5	0.256	25	J0449+1121
α Tau	2011 Feb 13	C	5.0	6.0	1.2	0.256	21	J0449+1121
α Tau	2011 Feb 12	S	3.1	9.5	1.8	0.256	11	J0431+2037

[a] Central frequency of selected bandpass.
[b] Number of available antennae remaining after flagging.

tennae. Visual inspection of each scan was carried out to determine if data at the beginning or end of these scans needed to be flagged. For the 2011 low frequency data the two sub-bands were centered at relatively radio frequency interference (RFI) free regions of the bandpass and only a very small amount of RFI had to be flagged. The 2012 wide-band data were initially Hanning smoothed (combining adjacent frequency channels with weights 0.25, 0.5, and 0.25) to suppress Gibbs ringing. We manually flagged entire sub-bands that were badly contaminated with RFI. The *testautoflag* task was then used to conservatively flag RFI from all sources and any remaining RFI was manually flagged.

In order to calibrate the data, we solved for the complex gains of the calibration sources while applying the bandpass solution, which was derived from the relevant aforementioned flux calibrators. The amplitude gains of the phase calibrators were scaled according to values derived from the flux calibrators using the "Perley-Butler 2010" flux density standard. At the time, no Ka or S-band flux density standard models were available so instead for these we used the K and L-band models, respectively. The more frequently observed phase calibrators were then used to calibrate the amplitude and phases of the targets. Atmospheric opacity corrections were also applied to the high frequency data sets using the average of a seasonal model (based on many years of measurements) and information from the weather station obtained during the observations.

The visibilities were then both Fourier transformed and deconvolved using the CASA *clean* task in multi-frequency synthesis imaging mode, which separately grids the the multiple spectral channels onto the *u-v* plane and therefore improves the overall *u-v* coverage. We used natural weighting for maximum sensitivity and the cell size was chosen so that the synthesized beam was about five pixels across. For the high frequencies it was usually sufficient to place just one CLEAN circle around the target source. For the low frequencies however, the image sizes were usually set to a few times the size of the primary beam so that nearby strong serendipitous sources could be CLEANed thus reducing their sidelobe contamination of the final image. These images were CLEANed interactively, with w-term correction, down

to about the 3σ level with clean boxes placed around sources as they appeared in the residual image. All images were corrected for primary beam attenuation.

In each image the flux density from the unresolved target source was calculated by, 1) taking the peak pixel value from the source, 2) manually integrating the flux density around the source, and 3) fitting an elliptical Gaussian model to the source and deriving the integrated flux density using the CASA *imfit* task. Each of these values along with the image root mean square (rms) noise measured from adjacent background regions and fitting error produced by *imfit* are given in Table 3. We assume absolute flux density scale systematic uncertainties of 3% at all frequencies (Perley & Butler 2013).

3. RESULTS

Apart from α Boo at C-band and α Tau at S-band, detections were made in both sub-bands for the 2011 data. At each other frequency, the flux densities of the targets in both sub-bands were found to be the same within their uncertainties so we do not present these values here. Instead we give the values from the radio maps produced by concatenating the two sub-bands. We present in Table 3 the target flux densities extracted from these concatenated radio maps. In the following two sections we briefly discuss the properties of these radio maps for both targets.

3.1. α Boo Radio Maps

High S/N detections ($> 19\sigma$) of α Boo were made at 22.5, 33.6, and 43.3 GHz. Some residuals of the dirty beam remained in the CLEANed maps due to the paucity of uv-coverage in these short high frequency observations. The lower frequencies maps were contaminated by the emission of a strong radio source located 186$''$ north-west of α Boo. This source was reported by Drake & Linsky (1986) and their flux density of 25 mJy at 4.9 GHz is in close agreement with our measurement of 23.2 mJy at the same frequency. We find the source to have a spectral index of -1.4 and reaches 80.3 mJy at 1.6 GHz. Surprisingly we do not detect α Boo in the higher frequency sub-band at 5.0 GHz (C-band) so the values given in Table 3 are taken from the lower frequency sub-band only. We obtain good detections ($> 5\sigma$) of the star for both

Table 3
VLA Fluxe Densities of α Boo and α Tau

	Band	Frequency[a] (GHz)	Peak F_ν (mJy)	Integrated F_ν (mJy)	*Imfit* Integrated F_ν (mJy)	Image rms (Jy beam^{-1})	*Imfit* Fitting Error (mJy)
α Boo (K2 III)	Q	43.28	5.941	6.093	6.420	0.301	0.261
	Ka	33.56	4.159	4.319	4.489	0.083	0.090
	K	22.46	1.827	1.784	1.809	0.043	0.050
	X	8.46	0.510	0.514	0.532	0.030	0.019
	C	4.90	0.214	0.144	0.159	0.035	0.009
	S	3.15	0.148	0.135	0.160	0.028	0.010
	S	2.87	0.127	0.118	0.116	0.012	0.016
	L	1.63	0.067	0.068	0.090	0.013	0.015
α Tau (K5 III)	Q	43.28	3.672	3.734	4.082	0.259	0.183
	Ka	33.56	2.188	1.962	2.125	0.091	0.070
	K	22.46	1.864	1.881	2.069	0.042	0.083
	X	8.46	0.296	0.287	0.281	0.014	0.015
	C	4.96	0.147	0.167	0.176	0.010	0.010
	S	3.15	0.062	0.043	-	0.017	-

[a] Frequency of the final image produced using the multi-frequency synthesis imaging mode within CASA's *clean* task.

epochs at $\sim$3 GHz (S-band) and the peak flux densities agree within their uncertainties. We can therefore safely assume that the 1.5 GHz (L-band) flux density has not changed significantly over that period either, and so can safely be included in any analysis. The map at L-band was highly contaminated by the sidelobes of the strong source north-west of α Boo but the star is still detected at the 5σ level. There is a slight positional offset of $1''$ between the position of the peak flux density at 1.5 and at 3.0 GHz for the 2012 data, which were taken within 1 day of each other. However, this is less than a quarter of the 1.5 GHz synthesized beam and considering that the 4σ contours overlap, we feel that it is highly unlikely that both sources are not α Boo.

3.2. α Tau Radio Maps

The final deconvolved radio maps of α Tau were of excellent quality with the rms noise reaching the predicted thermal noise in many cases. The target field at all frequencies was free from strong serendipitous radio sources and thus the final images were free of the sidelobe contamination that were present in the low frequency α Boo images. α Tau was the only source in the high frequency maps while the brightest source in the low frequency maps was located $106''$ north north-east of α Tau and had flux densities of 0.85, 1.35, and 1.7 mJy at 8.5, 5.0, and 3.5 GHz, respectively. Strong detections ($> 14\sigma$) of α Tau were made at all frequencies between 5.0 and 43.3 GHz. Due to the limited number of S-band receivers installed at the time, a full 2.5 hr track was dedicated to α Tau at 3.1 GHz in order to achieve the required sensitivity to give a possible detection. We report a tentative 3σ detection of α Tau at 3.1 GHz when we take its peak pixel value as its total flux density. As this is a weak detection we avoid using the *imfit* task to obtain a flux density estimate, as this may introduce additional errors (Taylor et al. 1999).

4. DISCUSSION

4.1. *Results Versus Previous Observations*

Prior to and during the early operation of the 'old' VLA, a small number of single dish radio observations reported the detection of flares from single red giants (e.g., Boice et al. 1981). These transient radio events

have never been re-observed however, even with more sensitive interferometers, suggesting that such detections were false (e.g., Beasley et al. 1992). The first definitive detection of thermal free-free emission from a luminosity class III single red giant at centimeter wavelengths was of α Boo at 6 cm (Drake & Linsky 1983, 1986). Since then there has been a modest number of sporadic centimeter and millimeter observations of this star. In Table 4 we list the majority of these observations and plot their flux densities as a function of frequency in Figure 1. In comparison to other single red giants, α Boo had been relatively well observed at radio wavelengths before this study, including detections in four VLA bands (i.e., Q, K, Ku, and C). No Ku band receivers were available during the commissioning phase of the VLA in early 2011 so we can compare three of our detections with previous ones.

Previous detections of α Boo at 6 cm ranged from a 3σ upper limit of 0.18 mJy to a 3σ detection at 0.39 mJy. Our 6 cm value agrees to within $\sim$10% of the highest S/N (5σ) value of Drake & Linsky (1986). There is no significant difference between our 1.3 cm value and that of Dehaes et al. (2011). There is however a notable difference in flux density values at 0.7 cm where Dehaes et al. (2011) report values that are lower than ours by over 40%. Such a level of chromospheric variability seems rather high and would be unexpected from such supposedly inactive stars. Another possibility for the difference in values is that the longer cycle time used by Dehaes et al. (2011), which was over double our value, may cause larger phase errors and thus lower final flux density values. Future high frequency VLA observations of α Boo will clarify this discrepancy at 0.7 cm but past detections at longer wavelengths appear to be in good agreement with our data.

Prior to this study, α Tau had only been detected at two VLA bands (i.e., X and Ku) and had never been detected at wavelengths longer than 3 cm due to its weakly ionized wind. The lack of a Ku measurement means that we can only compare the previous 3 cm detection of Brown & Harper (1997) to ours. We find that there is no significant difference between the two. Interestingly however, Brown & Harper (1997; priv. comm.) failed to detect α Tau at 6 cm but placed a 3σ upper limit of 0.07

Table 4
Compilation of Previous Radio Observations of α Boo and α Tau ($\nu \leq 250$ GHz)

	Frequency (GHz)	Date	Flux Density (mJy)	Source
α Boo (K2 III)	4.9	1983 Jan 21	0.39 ± 0.13	Drake & Linsky (1986)
	4.9	1983 May 20	0.26 ± 0.08	Drake & Linsky (1986)
	4.9	1983 Dec 26	$\leq 0.18(3\sigma)$	Drake & Linsky (1986)
	4.9	1984 Mar 17	0.24 ± 0.05	Drake & Linsky (1986)
	15.0	1984 Nov 6	0.68 ± 0.09	Drake & Linsky (1986)
	22.5	1999 Jan 06	1.7 ± 0.2	Dehaes et al. (2011)
	43.3	1999 Jan 06	3.3 ± 0.4	Dehaes et al. (2011)
	43.3	2004 Jan 25	3.34 ± 0.08	Dehaes et al. (2011)
	86.0	1985 Nov	21.4 ± 7.5	Altenhoff et al. (1986)
	108.4	1997 Nov - 2000 Jun	20.09 ± 0.69	Cohen et al. (2005)
	217.8	1997 Nov - 2000 Jun	83.5 ± 1.71	Cohen et al. (2005)
	250.0	1986 Dec - 1989 Mar	78 ± 8	Altenhoff et al. (1994)
α Tau (K5 III)	4.9	1983 Jan 21	$\leq 0.27(3\sigma)$	Drake & Linsky (1986)
	4.9	1984 Nov 6	$\leq 0.22(3\sigma)$	Drake & Linsky (1986)
	5.0	1997 Sep 27	$\leq 0.07(3\sigma)$	Wood et al. (2007)
	8.5	1997 Sep 27	0.28 ± 0.03	Wood et al. (2007)
	14.9	1997 Sep 27	0.95 ± 0.08	Wood et al. (2007)
	15.0	1984 Nov 6	0.60 ± 0.1	Drake & Linsky (1986)
	108.4	1997 Nov - 2000 Dec	13.97 ± 1.46	Cohen et al. (2005)
	217.8	1999 Sep - 2000 Dec	25.78 ± 5.64	Cohen et al. (2005)
	250.0	1986 Dec - 1987 Jan	51 ± 6	Altenhoff et al. (1994)

mJy on its emission. In stark contrast to this, we were able to detect the star at 6 cm with a flux density over two times greater than this value. This hint of variability at long wavelengths can only again be confirmed with future high S/N observations.

4.2. *Existing Atmospheric Models*

GMH: A few words on Radspec code.

One of the most important diagnostic features indicating mass outflows in late type stars are the blue shifted absorption components present in the Mg II h and k resonance lines. Figure 1 shows the predicted radio spectrum from the chromosphere and wind models of Drake (1985), which were based on the Mg II k 2796 Å emission line taken with the the International Ultraviolet Explorer. Both of Drake's models predict the wind to reach a terminal velocity, v_∞, of 40 km s^{-1} at ~ 2 $R_\star$ and have a broad temperature plateau with T $\approx 8,000$ K between 1.2 and ~ 13 $R_\star$ with a cooler region further out. At high frequencies the radio spectra produced by these models have a blackbody-like slope (i.e., $\sim \nu^2$) as a result of the small density scale heights close to the star. At low frequencies however, where the models predict the wind to have constant velocity, ionization and temperature, the slopes approaches the well known $\sim \nu^{0.6}$ limit (Wright & Barlow 1975; Olnon 1975; Panagia & Felli 1975). The paucity and, in some cases low S/N, of previous observations made it difficult to discern the validity of this model prior to our multi-frequency study of α Boo. Our new data reveal significant deviations from the current existing semi-empirical model at both low and high frequencies (in this case below ~ 8 GHz and above ~ 25 GHz). At high frequencies our VLA data indicates a flux excess which is in agreement with previous mm-observations. The discrepancy at low frequencies may indicate that we are still sampling a region of the wind where it is still accelerating (i.e., it has not yet reached its terminal velocity) or may also be a manifestation of rapid wind cooling further out than that predicted in UV spectral

analysis. We will discuss these possibilities in the following sections.

In Figure 2 we plot the expected radio spectrum of α Tau based on the semi-empirical 1-D chromospheric model of McMurry (1999) embedded in the 1-D wind model of Robinson et al. (1998). The McMurry model includes a transition region and reaches a maximum temperature of 10^5 K at 1.2 $R_\star$. Beyond 1.2 $R_\star$ we use Robinson's wind characteristics to describe the outflow velocity where the wind reaches $\sim 80\%$ of its terminal value by 3 $R_\star$. We assume the wind to have a constant temperature of 8,000 K and have a constant ionization fraction, x_e, of 0.01 throughout. The combination of both atmospheric models result in a predicted excess of radio flux density at high frequencies (i.e., $>$ 30 GHz) but does a good job in reproducing the VLA flux densities below 30 GHz. The VLA, Institut de Radioastronomie Millimétrique (IRAM) 30 m-telescope and Berkeley Illinois Maryland Association (BIMA) continuum fluxe densities confirm that this model predicts a flux excess at even higher frequencies. One possible explanation for this is that the inner atmosphere contains extensive cooler gas than that predicted by the 1-D static chromospheric model of McMurry. This scenario agrees with the findings of Wiedemann et al. (1994) who conclude that cool regions exist close to the stellar surface with large filling factors i.e., a thermally bifurcated CO-mosphere. For α Boo there is a hint that the transition frequency between wind and chromosphere occurs at about 8.5 GHz due to the change of slope but for α Tau, with its low mass loss rate giving rise to a low wind opacity, this is harder to distinguish. There is a small hint that this may occur at 6 cm and a higher S/N detection at 13 cm would confirm this.

We also include the predicted radio spectrum from the theoretical Alfvèn wave driven outflow model for α Tau (Krogulec 1989) in Figure 2 to demonstrate how radio observations can test the robustness of theoretical models. This model is based on a larger than now expected
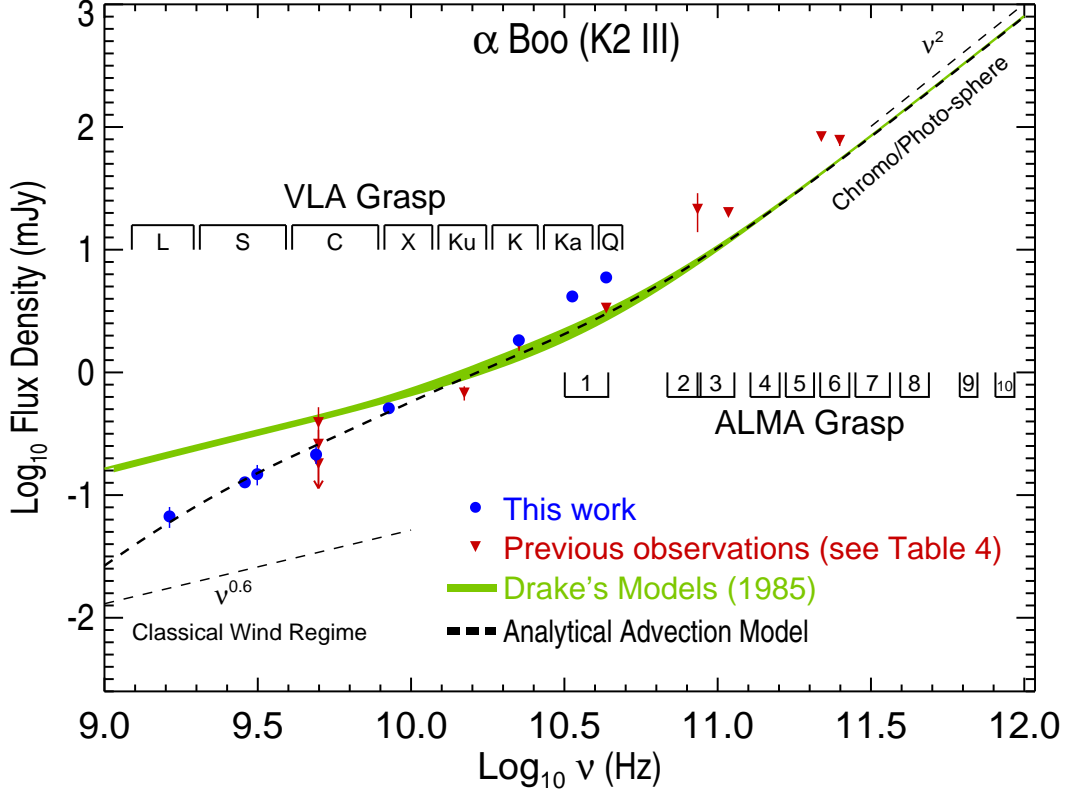
Figure 1. Spectral energy distribution of α Boo for 1 GHz $\leq \nu \leq$ 1 THz. Our new multi-frequency VLA observations which were mainly acquired over a few days in February 2011 are the blue circles and are in disagreement with the existing chromospheric and wind models of Drake (1985). The overlap between the two models are represented by the green shaded area. The red triangles are previous observations which were acquired sporadically over the past $\sim$ 25 years with the 'old' VLA, IRAM and BIMA. The black dashed line is the expected radio emission from the Drake model which undergoes rapid wind cooling beyond $\sim$2.3 $R_\star$ (see Section 4.3 and 4.4).
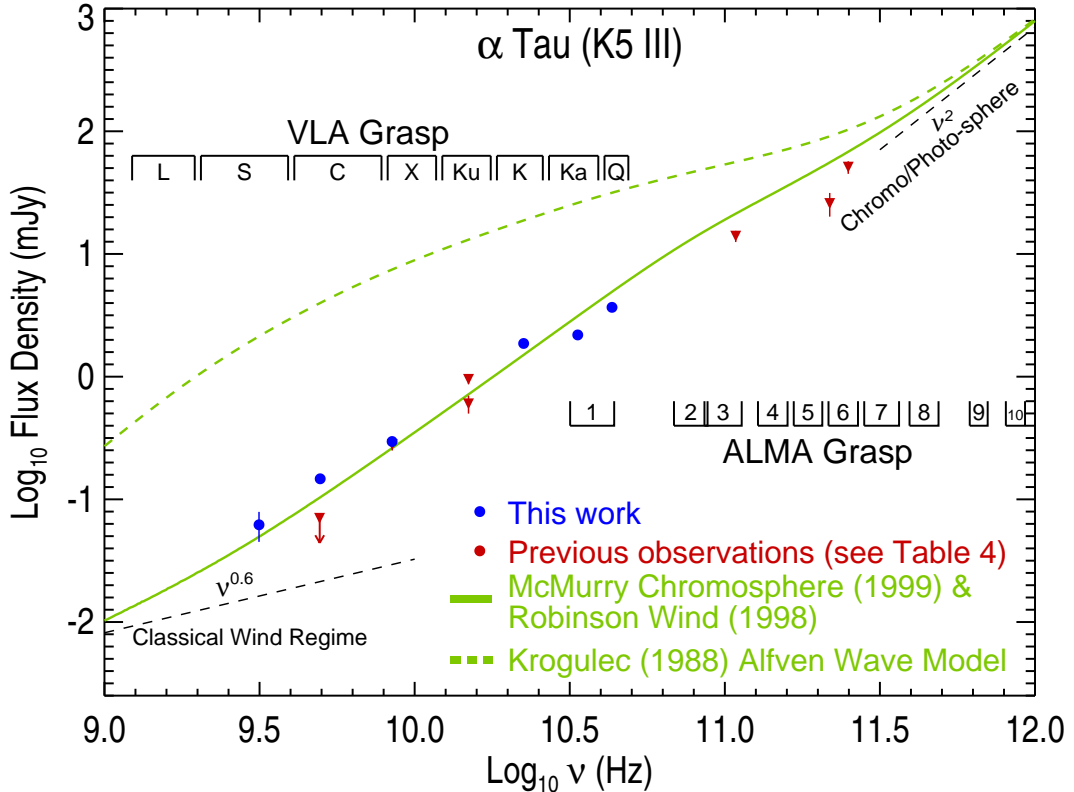
Figure 2. Spectral energy distribution of α Tau for 1 GHz $\leq \nu \leq$ 1 THz. All our new multi-frequency VLA observations of α Tau (blue circles) were acquired in just two days in February 2011. The red triangles are the previous radio observations of the star which were acquired over many years. The green line is the expected radio emission from the current hybrid chromosphere and wind model while the dashed green line is the expected radio emission from a theoretical Alfvèn wave driven model atmosphere.
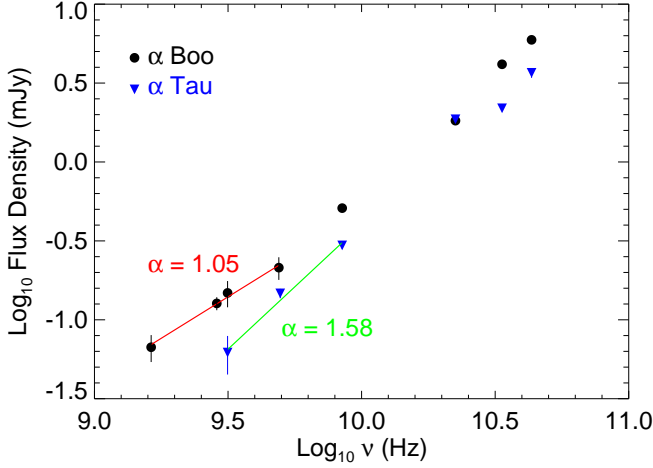
Figure 3. Radio spectra for α Boo and α Tau, together with the best fit straight lines to their long wavelength flux densities and the resulting spectral indices.
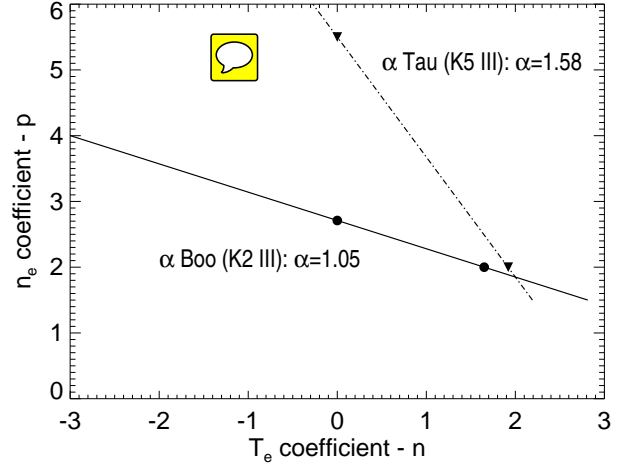

Figure 4. The variation of density and temperature coefficients for the empirically derived spectral indices. The density coefficients for an isothermal flow along with the temperature coefficients for a constant outflow velocity are also shown for both stars.

mass loss rate for the star (i.e., 6.3×10^{-9} M$_\odot$ yr^{-1}) and predicts a fully ionized outflow with $v_\infty \approx 115$ km s^{-1}. As the radio opacity is proportional to $n_e n_{ion}$ this model greatly overestimates the actual radio flux density at all VLA wavelengths. The same result is to be expected from the Alfvèn wave models of α Boo (Krogulec 1988) which are also fully ionized and have larger than now expected mass loss rates and outflow velocities.

4.3. Radio Spectral Indices

For a thermal source which has a constant electron density distribution, its radio emission has a well defined spectral index α ($F_\nu \propto \nu^\alpha$). For an optically thick homogeneous plasma α follows the Rayleigh-Jeans tail of the Planck function (i.e., $\alpha = +2$), while for an optically thin plasma $\alpha = -0.1$. However, the electron density in the mass outflow region of a star is not constant as a function of radius and varies by many orders of magnitude. It can be shown that the expected radio spectrum from an isothermal spherically symmetric steady flow varies as $\nu^{0.6}$ (Wright & Barlow 1975; Olnon 1975; Panagia & Felli 1975). If we relax some of these assumptions about the outflow and instead assume that the electron density and temperature profiles vary as a function of distance from the star r, and have the form $n_e \propto r^{-p}$ and $T_e \propto r^{-n}$ respectively, then

$$\alpha = \frac{4p - 6.2 - 0.6n}{2p - 1 - 1.35n} \qquad (1)$$

(e.g., Seaquist & Taylor 1987). Here $p > 1.5$, otherwise we are in the optically thin regime. Equation 1 is also only valid if the ionization fraction is constant throughout the outflow. By making these assumptions and assuming either a constant velocity (i.e., $p = 2$) or an isothermal outflow (i.e., $n = 0$), we can easily estimate the power-law decay of either the temperature or velocity profile, respectively.

The radio spectra for both stars are shown in Figure 3, together with the straight lines that were fitted to the long wavelength flux densities by minimizing the chi-square error statistic. For α Boo a straight line with

$F_\nu \propto \nu^{1.05 \pm 0.05}$ fits the four longest wavelength data points well. This spectral index is larger than the 0.8 value obtained by Drake & Linsky (1986) whose value was based on a shorter wavelength (2 cm) value and a mean value of four low S/N measurements at 6 cm. α Tau was found to have a larger spectral index and a straight line with $S_\nu \propto \nu^{1.58 \pm 0.25}$ best fitted the three longest wavelength data points. This value is in agreement with Drake & Linsky (1986) who report a value ≥ 0.84 and is lower than the value of 2.18 that can be derived from the shorter wavelength data given in Wood et al. (2007). It should be emphasized that the spectral index for both stars is steeper than that expected for an isothermal spherically symmetric steady flow.

Equation 1 can be used in conjunction with our new spectral index for each star to calculate possible density and temperature coefficients that describe their outflow. The degree of variation of these coefficients with respect to one another is shown in Figure 4. A common explanation in the literature for spectral indices of stellar outflows being larger than 0.6 is that the wind is still accelerating in the region where the radio emission is emanating from and thermal gradients are usually ignored. If we too make this assumption then the density coefficients are 2.71 and 5.5 for α Boo and α Tau, respectively. This assumption is reasonable at short wavelengths where the majority of the radio emission is expected to emanate within the wind's acceleration zone, but at long VLA wavelengths (i.e., between 6 and 20 cm) this assumption may be false and we may indeed be sampling the wind very close to or at its terminal velocity.

To investigate this matter further, we estimate the effective radius of the radio emitting region per wavelength based on the Drake model for α Boo and the hybrid McMurry and Robinson model for α Tau. We follow the approach used by Cassinelli & Hartmann (1977) and assume that the radio emission at each wavelength emanates from a surface at radial optical depth $\tau_{rad} = 1/3$. This is just the Eddington-Barbier relation for an extended atmosphere where emission from smaller optical depths gets added weight. Since the radio free-free
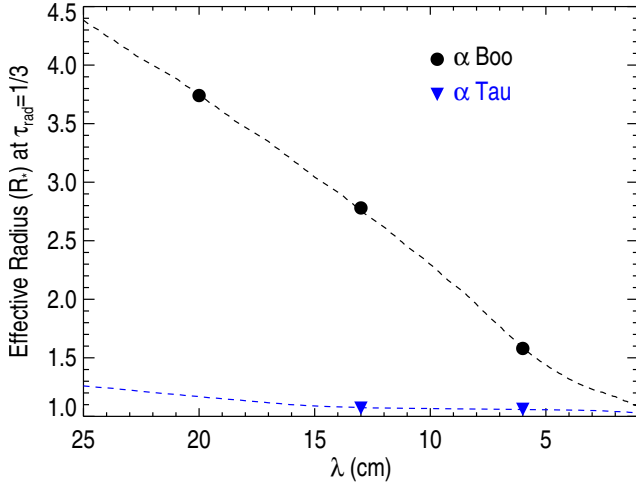
Figure 5. Predicted effective radius (dashed lines) as a function of wavelength for α Boo and α Tau. Points corresponding to our long wavelength VLA measurements are also shown. At the same radio wavelengths the less ionized mass outflow of α Tau results in a smaller effective radius than α Boo.

opacity increases at longer wavelengths (i.e., $\kappa_\lambda \propto \lambda^{2.1}$) the optical depth along a line of sight into the stellar outflow also increases at longer wavelengths. This implies that the effective radius (i.e., the radius where $\tau_\lambda = \tau_{\rm rad}$) will increase with longer wavelengths and will be greater for outflows with higher ionization densities as $\tau_\lambda \propto \int \lambda^{2.1} n_{\rm ion} n_e dr$.

The higher degree of ionization in the mass outflow of α Boo in comparison to α Tau makes a substantial difference to the size of the stars effective radius as can be seen in Figure 4. At 6, 13, and 20 cm the effective radius of α Boo at $\tau_{\rm rad}=1/3$ is predicted to be 1.6, 2.8, and 3.7 $R_\star$ but is only $\sim$1.1 $R_\star$ at 6 and 13 cm for α Tau. Robinson et al. (1998) predict that α Tau's wind reaches $\sim$80% of its terminal velocity by 3 $R_\star$ so it is highly unlikely that even our longest wavelength VLA measurements of α Tau sample its outer wind. For α Boo however, Drake (1985) predicts that the wind has reached its terminal velocity by $\sim$2 $R_\star$ so based on this model our longest VLA measurements probable sample the wind at, or very close to, its terminal velocity. Assuming this to be the case, Equation 1 then indicates that α Boo's steady outflow undergoes rapid cooling at a few stellar radii. The derived temperature coefficient of 1.65 points to a temperature power-law falloff exceeding that from a wind adiabatically cooling with no heat source (i.e. n=4/3 in this case) with the excess cooling being possible due to recombination of H$^+$ or heavier ions. Finally, if the wind ionization balance has not yet become *frozen-in* in the region of Boo's wind where the radio emission emanates from then the excess slope of the spectral index could be due to a combination of both cooling and changing ionization balance. In this scenario the temperature coefficient may be smaller then our derived value here.

4.4. Analytical Advection Model for α Boo's Wind

A failure of the existing atmospheric model for α Boo is that is overestimates the radio fluxes at long VLA wavelengths which sample its outer atmosphere, as clearly shown in Figure 1. If these wavelengths are indeed sam-

pling the wind at its terminal velocity then a reason for this overestimation may be that the wind is cooling closer in than that predicted by the existing model, which assumes a constant temperature of 8,000 K out to $\sim$10 $R_\star$. The main mechanism for this cooling would be adiabatic expansion (O'Gorman & Harper 2011) and would cause lower electron densities than those predicted by the existing model due to larger recombination rates. To investigate this possibility further we adjusted the existing model to include a temperature power-law falloff of the form

$$T_e(r) = T_e(r_1)\left(\frac{r_1}{r}\right)^{1.65}, \qquad (2)$$

at some distance r_1, from the star. The temperature coefficient is that obtained from our new VLA data assuming a steady flow (see Figure 4). To calculate the new n_e and $n_{\rm ion}$ densities in the wind regime where this temperature falloff occurs, we used the analytical expression of Glassgold & Huggins (1986) to calculate the hydrogen ionization fraction, $x_{\rm H} = n_{\rm HII}/n_{\rm H}$. In doing so we need to make a number of assumptions about the wind properties from r_1 onwards.

1. We assume a conserved mass outflow i.e., $n_{\rm H}(r) = C/r^2$ where $n_{\rm H}$ is the total hydrogen number density and C is a constant proportional to the ratio of the mass loss rate divided by the terminal velocity. For α Boo, $C = 1.5 \times 10^{32}$ cm^{-1}.

2. We assume that all ionization processes cease (**GMH**).

3. We consider only radiative recombination of H and include the temperature variation of the recombination coefficient α_b which excludes captures to the n=1 level (Spitzer 1978). The recombination coefficient varies with temperature according the the relationship

$$\alpha_b = \alpha_b(r_1)\left[\frac{T(r_1)}{T(r)}\right]^{0.77}, \qquad (3)$$

where the power law coefficient is obtained by finding the slope of the best fit line through the recombination coefficients between 1,000 K and 16,000 K defined in Spitzer (1978).

4. We assume a constant heavy ion fraction, $x_{\rm ion} = n_{\rm ion}/n_{\rm H} = 10^{-4}$.

Using these assumptions it can be shown that the ionization fraction beyond r_1 is given by

$$x_{\rm H}(r) = \frac{x_{\rm H}(r_1)x_{\rm ion}e^{-I(r)}}{x_{\rm ion} + x_{\rm H}(r_1)[1 - e^{-I(r)}]} \qquad (4)$$

where

$$I(r) = 2.38 \times 10^{-3}\left[\left(\frac{r_1}{r}\right)^{-0.19} - 1\right], \text{ and } r \geq r_1. \quad (5)$$

By altering the existing atmospheric model so that it now has a narrow temperature plateau of $T_e = 10,000$ K between 1.2 and 2.3 $R_\star$, a temperature profile and a density profile governed by given by Equation 2 and Equation 4 beyond 2.3 $R_\star$ respectively, then we get good agreement with our new long wavelength VLA data as shown in Figure 1. This new *hybrid* model, which still has the original ionization fraction of $x_{\rm H} \approx 0.5$ inside

2.3 $R_\star$, now contains an initial rapid decrease in x_H post 2.3 $R_\star$ which then tails off to a constant value of ~0.04 beyond $\sim10R_\star$.

Encouraging as it is that such a simple analytical model can reproduce values close to the observed radio fluxes at long wavelengths, it must be stressed that this *hybrid* model is just a first order approximation. It assumes that the excess slope from the radio spectrum is a result of rapid cooling alone. It still does not reproduce the radio fluxes at wavelengths shorter than ~3 cm and therefore a new atmospheric model is still required that can reproduce all of the observed fluxe densities. To do so, the non-trivial task of simultaneously solving the non-local radiative transfer equation and atomic rate equations which include advection will be required.

5. CONCLUSIONS

We have presented the most comprehensive set of multi-wavelength radio continuum observations of two standard luminosity class III red giants to date. This is the first time such classes of stars have been detected longword of 6 cm. Such long wavelength detections are crucial if one wants to study the outer environments of these partially ionized stellar outflows. Our observations were carried out with the VLA during its commissioning phase when only a fraction of the now available bandwidth was at our disposal. The continuous bandwidth coverage between 1 and 50 GHz of the new VLA will allow fast detections of historically weak or undetectable radio continuum luminosity class III red giants at both long and short wavelengths. Previous upper limits will be replaced by firm detections allowing a greater understanding of their atmospheric properties.

The spectral index of both α Tau and α Boo at long wavelengths is found to be greater than the predicted value for an isothermal steady spherically symmetric flow. For α Tau our longest wavelength detections are still sampling emission from an accelerating region within the outflow while for α Boo the emission probably emanates from a region where the flow is close to, or indeed have reached its terminal velocity. We have developed a simple analytical model for the outer atmosphere of α Boo based on these measurements which contains a rapid wind cooling profile. Future detailed non-LTE radiative transfer models which include advection are required to match all radio flux densities at all wavelengths.

REFERENCES

Altenhoff, W. J., Huchtmeier, W. K., Schmidt, J., Schraml, J. B., & Stumpff, P. 1986, A&A, 164, 227

Altenhoff, W. J., Thum, C., & Wendker, H. J. 1994, A&A, 281, 161

Ayres, T. R., Linsky, J. L., Vaiana, G. S., Golub, L., & Rosner, R. 1981, ApJ, 250, 293

Baade, R., Kirsch, T., Reimers, D., Toussaint, F., Bennett, P. D., Brown, A., & Harper, G. M. 1996, ApJ, 466, 979

Beasley, A. J., Stewart, R. T., & Carter, B. D. 1992, MNRAS, 254, 1

Boice, D. C., Kuhn, J. R., Robinson, R. D., & Worden, S. P. 1981, ApJ, 245, L71

Carpenter, K. G., Robinson, R. D., Harper, G. M., Bennett, P. D., Brown, A., & Mullan, D. J. 1999, ApJ, 521, 382

Cassinelli, J. P., & Hartmann, L. 1977, ApJ, 212, 488

Chapman, R. D. 1981, ApJ, 248, 1043

Cohen, M., Carbon, D. F., Welch, W. J., Lim, T., Schulz, B., McMurry, A. D., Forster, J. R., & Goorvitch, D. 2005, AJ, 129, 2836

Crowley, C., Espey, B. R., Harper, G. M., & Roche, J. 2009, in American Institute of Physics Conference Series, Vol. 1094, 15th Cambridge Workshop on Cool Stars, Stellar Systems, and the Sun, ed. E. Stempels, 267–274

Crowley, C., Espey, B. R., & McCandliss, S. R. 2008, ApJ, 675, 711

Dehaes, S., et al. 2011, A&A, 533, A107

di Benedetto, G. P. 1993, A&A, 270, 315

Drake, S. A. 1985, in Progress in stellar spectral line formation theory; Proceedings of the Advanced Research Workshop, Trieste, Italy, September 4-7, 1984 (A86-37976 17-90). Dordrecht, D. Reidel Publishing Co., 1985, p. 351-357., ed. J. E. Beckman & L. Crivellari, 351–357

Drake, S. A., & Linsky, J. L. 1983, ApJ, 274, L77

—. 1986, AJ, 91, 602

Eaton, J. A. 2008, AJ, 136, 1964

Falceta-Gonçalves, D., Vidotto, A. A., & Jatenco-Pereira, V. 2006, MNRAS, 368, 1145

Glassgold, A. E., & Huggins, P. J. 1986, ApJ, 306, 605

Harper, G. M. 2010, ApJ, 720, 1767

Harper, G. M., Brown, A., Bennett, P. D., Baade, R., Walder, R., & Hummel, C. A. 2005, AJ, 129, 1018

Hartmann, L., & MacGregor, K. B. 1980, ApJ, 242, 260

Holzer, T. E., & MacGregor, K. B. 1985, in Astrophysics and Space Science Library, Vol. 117, Mass Loss from Red Giants, ed. M. Morris & B. Zuckerman, 229–255

Judge, P. G., & Carpenter, K. G. 1998, ApJ, 494, 828

Krogulec, M. 1988, , 38, 107

—. 1989, , 39, 51

Linsky, J. L., & Haisch, B. M. 1979, ApJ, 229, L27

McMullin, J. P., Waters, B., Schiebel, D., Young, W., & Golap, K. 2007, in Astronomical Society of the Pacific Conference Series, Vol. 376, Astronomical Data Analysis Software and Systems XVI, ed. R. A. Shaw, F. Hill, & D. J. Bell, 127

McMurry, A. D. 1999, MNRAS, 302, 37

O'Gorman, E., & Harper, G. M. 2011, in Astronomical Society of the Pacific Conference Series, Vol. 448, 16th Cambridge Workshop on Cool Stars, Stellar Systems, and the Sun, ed. C. Johns-Krull, M. K. Browning, & A. A. West, 691

Olnon, F. M. 1975, A&A, 39, 217

Panagia, N., & Felli, M. 1975, A&A, 39, 1

Perley, R. A., & Butler, B. J. 2013, ApJS, 204, 19

Robinson, R. D., Carpenter, K. G., & Brown, A. 1998, ApJ, 503, 396

Seaquist, E. R., & Taylor, A. R. 1987, ApJ, 312, 813

Spitzer, L. 1978, Physical processes in the interstellar medium

Sutmann, G., & Cuntz, M. 1995, ApJ, 442, L61

Suzuki, T. K. 2007, ApJ, 659, 1592

Taylor, G. B., Carilli, C. L., & Perley, R. A., eds. 1999, Astronomical Society of the Pacific Conference Series, Vol. 180, Synthesis Imaging in Radio Astronomy II

van Leeuwen, F. 2007, A&A, 474, 653

Wiedemann, G., Ayres, T. R., Jennings, D. E., & Saar, S. H. 1994, ApJ, 423, 806

Wood, B. E., Harper, G. M., Müller, H.-R., Heerikhuisen, J., & Zank, G. P. 2007, ApJ, 655, 946

Wright, A. E., & Barlow, M. J. 1975, MNRAS, 170, 41